Elastic and inelastic scattering of ^{16}O and ^{18}O ions from ^{64}Zn at energies near the Coulomb barrier

S. Salém-Vasconcelos, E.M. Takagui, M.J. Bechara, K. Koide, and O. Dietzsch
Instituto de Física, Universidade de São Paulo, São Paulo, Brazil

A. Bairrio Nuevo, Jr.
Instituto de Física, Universidade Federal do Rio de Janeiro, Rio de Janeiro, Brazil

H. Takai
Brookhaven National Laboratory, Upton, New York 11973
(Received 20 December 1993)

Coulomb-nuclear interference effects were investigated in the inelastic scattering of ^{16}O and ^{18}O by ^{64}Zn. Measurements of elastic and inelastic angular distributions of ^{18}O were performed at a laboratory energy of 49 MeV, over the angular range from $\theta_{lab} \sim 30°$ to 85°. The excitation functions of ^{16}O and ^{18}O ions were measured at incident energies between 29 and 46 MeV at $\theta_{lab} = 174°$. The experimental angular distributions show structures which are more pronounced for projectile excitation than for target excitation. The interference minimum for the excitation of the ^{18}O first 2^+ state was found to be shifted towards forward angles by approximately 5°(c.m.) with respect to the distorted-wave Born approximation calculations and by approximately 3.5°(c.m.) with respect to the coupled-channels calculations. A pronounced Coulomb-nuclear interference minimum was seen in the excitation of $^{64}Zn(2^+)$ state by inelastic scattering of ^{16}O projectiles, whereas no pronounced minimum was observed in target excitation by ^{18}O projectiles. The elastic scattering data were analyzed with the optical model. The inelastic differential cross sections for the excitation of the first 2^+ states in the target and in the ^{18}O projectile were analyzed using the distorted-wave Born approximation and also the coupled-channels approach with collective form factors.

PACS number(s): 25.70.−z, 27.50.+e

I. INTRODUCTION

At energies in the vicinity of the Coulomb barrier both the Coulomb and the nuclear interactions play an important role for processes like inelastic scattering, which occur at the surface of the colliding nuclei. The interference between Coulomb and nuclear amplitudes shows typically a minimum in the inelastic cross-section angular distributions and excitation functions. This Coulomb-nuclear interference has been relatively well described by the distorted-wave Born approximation (DWBA) [1] with collective form factors for the excitation of low-lying 2^+ and 3^- collective states in several target nuclei, when there is no excitation of the projectile.

However, "anomalies" have been observed in inelastic scattering excitation functions and angular distributions for several systems when the projectile is excited [2–10]. In particular, for colliding systems in which the ^{18}O projectile is excited to the 2^+ state ($E_x = 1.98$ MeV), DWBA calculations using the collective model fail to describe the projectile excitation. In such cases, the experimental cross-section minimum resulting from the Coulomb-nuclear interference is usually shifted (3° – 6°) towards forward angles when compared to DWBA predictions. Such results, observed since early studies [2–6], still are not completely understood.

In an extension to higher bombarding energies of our earlier study [11] on the excitation of the first 2^+ excited state in ^{64}Zn, we have made detailed measurements of elastic and inelastic angular distributions and excitation functions for the scattering of ^{16}O and ^{18}O by ^{64}Zn, in the vicinity of the Coulomb barrier. We present here the experimental results and the analysis performed with DWBA and coupled-channels formalisms. We also present a comparison between projectile and target excitation in the $^{18}O + {}^{64}Zn$ system, and discuss the differences between the excitation of ^{64}Zn by ^{16}O and ^{18}O.

II. EXPERIMENTAL METHOD

Beams of ^{16}O and ^{18}O ions were extracted from a duoplasmatron ion source and accelerated in the electrostatic accelerator at the University of São Paulo. Beam currents measured in a Faraday cup after the target were of the order of 200 nA. The targets were made by vacuum evaporation of ZnO, enriched to 99.85% in ^{64}Zn, on a thin layer (~ 5 $\mu g/cm^2$) of Au evaporated onto 15 $\mu g/cm^2$ carbon backing. The ^{64}Zn targets were typically ~ 10 $\mu g/cm^2$. The Au layer was used in order to improve the uniformity of the deposited Zn layer in the evaporation process. It also served as a reference in the determination of the absolute cross sections.

Two different experimental setups were used to measure angular distributions and excitation functions. The excitation functions were measured in a 60 cm diameter scattering chamber [12] for incident beam energies in the vicinity of the Coulomb barrier, in 0.5 MeV steps.

The scattered ions were detected at $\theta_{lab} \sim 174°$ in a cooled ($\sim -30\,°$ C) annular silicon surface-barrier detector. Two silicon detectors symmetrically placed with respect to the beam direction at $\theta_{lab} = 30°$ were used to normalize the cross sections to absolute values and to monitor the beam direction. The energy resolution, essentially due to the target thickness, was $\sim$ 120 keV. At some energies $^{18}O+^{64}Zn$ spectra were contaminated by alpha particle groups from the $^{12}C(^{18}O, \alpha)^{26}Mg$ reaction on the carbon backing. This was the only source of discrete background which had to be considered in the analysis. For the spectra where the alpha and the inelastic peaks were partially resolved, the alpha background was subtracted by a peak fitting procedure using the experimental shape of an isolated alpha peak as a standard. Spectra in which the alpha group could not be separated from the peak of interest were not included in the present analysis. No background corrections were necessary for one and two neutron transfer reactions: (^{18}O,^{17}O) and (^{18}O,^{16}O). At the backward angle of 173.8°, due to the Q values involved, the ^{16}O, ^{17}O, and ^{18}O groups could be separated from each other. The contribution of ^{17}O and ^{65}Zn excited states from one neutron transfer reaction to the inelastic ^{64}Zn and ^{18}O peaks is negligible. Their contribution to the elastic ^{18}O peak is always less than 1% from estimates based on spectra taken at more forward angles with the magnetic spectrograph (see below) where mass identification was made. Also due to the Q values involved no background corrections from transfer reactions were necessary for the ^{16}O scattering spectra. Typical spectra are shown in Figs. 1 and 2. The spectra were analyzed using the method and the line-shape fitting program described in Refs. [13] and [14].

For the angular distribution measurements, a split-pole magnetic spectrograph [15, 16] was employed. The scattered ions were detected in a gas-filled E-ΔE position sensitive detector with a delay line readout [17, 18], placed in the focal plane of the spectrograph. The position resolution, corresponding to an energy resolution of approximatelly 140 keV, is mainly due to target thickness, and was adequate to completely resolve the

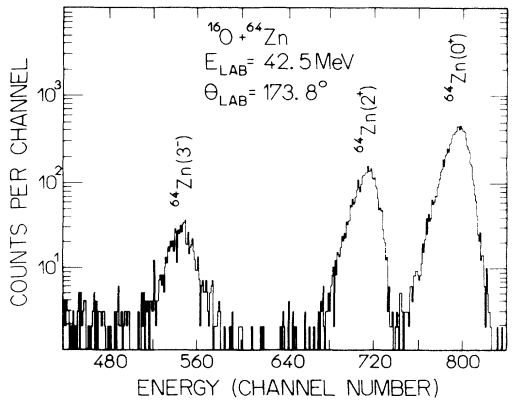

FIG. 1. Spectrum of backscattered particles from the elastic and inelastic collision of ^{16}O with ^{64}Zn at E_{lab} = 42.5 MeV, measured with a cooled annular surface barrier silicon detector.

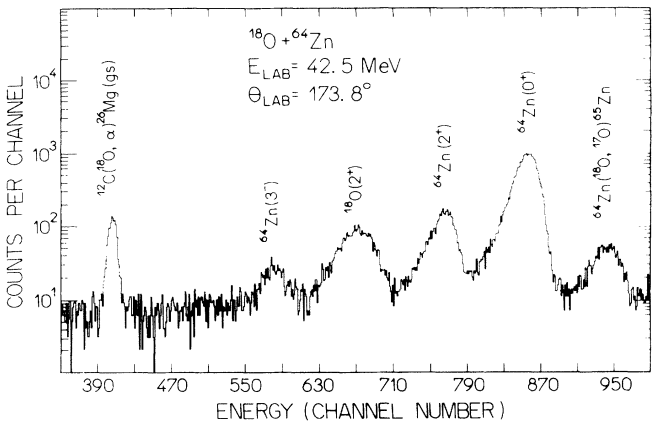

FIG. 2. Spectrum of backscattered particles from the elastic and inelastic collision of ^{18}O with ^{64}Zn at E_{lab} = 42.5 MeV, measured with a cooled annular surface barrier silicon detector.

inelastic groups. Three parameter data (particle energy E, partial energy loss ΔE, and particle position P along the focal plane) were stored in the computer and were recorded event by event on magnetic tapes for off-line analysis. The simultaneous determination of E, ΔE, and P allowed for a clear separation of masses 16, 17, and 18 of the oxygen ions. In particular, $^{64}Zn(^{18}O,^{17}O)^{65}Zn$ reaction products could be separated from the inelastic groups under study. A typical two-dimensional plot of E versus P is shown in Fig. 3. Groups of detected particles (A = 16, 17, and 18) are clearly separated from each other. The projected position spectrum for the ^{18}O group is presented in Fig. 4. Two silicon detectors symmetrically placed at $\theta_{lab} = 30°$ with respect to the beam

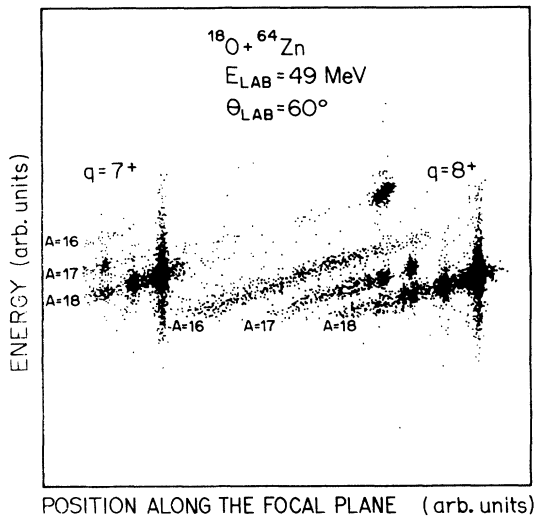

FIG. 3. Mass identification of products from ^{18}O + ^{64}Zn at E_{lab} = 49 MeV, measured with a position sensitive gas detector at the focal plane of the magnetic spectrograph at $\theta_{lab} = 60°$. Groups of particles corresponding to masses 16, 17, and 18 are clearly separated. Two charge states ($q = 7^+$ and $q = 8^+$) are detected in the range of magnetic rigidities covered by the detector.

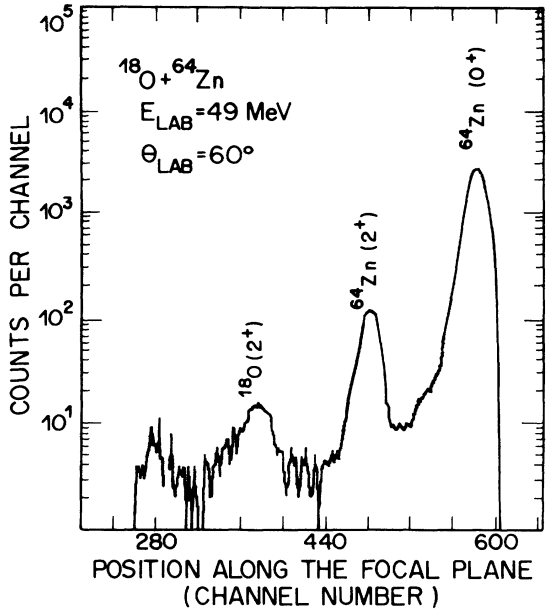

FIG. 4. Projected position spectrum for the ^{18}O group extracted from the two-dimensional spectrum presented in Fig. 3.

line were also used to monitor the beam direction and to normalize the cross sections to absolute values.

Due to charge separation in the magnetic spectrograph and because all charge states cannot be simultaneously detected in the position sensitive detector, the relative yields of the several charge states were measured in order to obtain the cross section values. The distributions for charge states 5^+, 6^+, 7^+, and 8^+ were determined by measuring the elastic scattering over the angular range $30° < \theta_{lab} < 85°$. The contribution from the 6^+, 7^+, and 8^+ charge states ranged from $\sim$ 15% to 30%, $\sim$ 45% to 50%, and $\sim$ 20% to 40%, respectively, depending on the energy of the outgoing ion. The contribution from the 5^+ charge state was always less than 3%.

The experimental angular distributions and excitation functions are presented in Figs. 5–7. The circles are experimental data and the error bars represent statistical uncertainties only. The curves are the results of theoretical calculations with the optical-model code ABACUS-3 [19] and with the heavy-ion program PTOLEMY [20] in its version [21,22] which can compute inelastic scattering cross sections in the DWBA or with the coupled-channels formalisms, as will be discussed in the next section.

III. THEORETICAL ANALYSIS

The elastic scattering differential cross sections were fitted by an optical-model analysis with a complex potential of Woods-Saxon geometry:

$$U(r) = -Vf(r) - iWg(r) + V_C(r), \tag{1}$$

where

$$f(r) = \left[1 + \exp\frac{(r-R)}{a}\right]^{-1}, \tag{2}$$

$$g(r) = \left[1 + \exp\frac{(r-R')}{a'}\right]^{-1}, \tag{3}$$

$$R = r_0\left(A_1^{1/3} + A_2^{1/3}\right), \tag{4}$$

$$R' = r_0'\left(A_1^{1/3} + A_2^{1/3}\right), \tag{5}$$

$$V_C(r) = \begin{cases} Z_1Z_2e^2/r & \text{for } r \geq R_C, \\ \frac{Z_1Z_2e^2}{2R_C}\left(3 - \frac{r^2}{R_C^2}\right) & \text{for } r < R_C, \end{cases} \tag{6}$$

$$R_C = 1.25\left(A_1^{1/3} + A_2^{1/3}\right), \tag{7}$$

with the mass number and the atomic number of the projectile and of the target designated by (A_1, Z_1) and (A_2, Z_2), respectively.

For each projectile several independent searches of optical parameters were done. The optical parameters for the $^{18}O+^{64}Zn$ system were initially determined by fitting the elastic scattering angular distribution with the code ABACUS-3 [19]. The final calculations were performed with the heavy-ion program PTOLEMY [20–22]. For the $^{16}O+^{64}Zn$ system the optical-model parameters were obtained by fitting the elastic scattering excitation function using the program PTOLEMY. Whenever available, values from the literature were used as initial sets. Several families of potentials that resulted in satisfactory fits to the elastic scattering data were obtained from starting parameter values taken from previous reports for the ^{16}O + ^{64}Ni system [2, 23, 24] and the $^{18}O+^{64}Ni$ system [2, 4]. Due to strong absorption, the different families of potentials produce the same elastic scattering. Additional information from inelastic data was used to remove the ambiguities in the optical potential.

The DWBA calculations were made with the heavy-ion computer code PTOLEMY [20–22]. A form factor $F_L(r)$ consisting of a Coulomb and a nuclear part was used to describe the inelastic excitation:

$$F_L(r) = F_L^C(r) + F_L^N(r). \tag{8}$$

The Coulomb part is given by

$$F_L^C(r) = \begin{cases} \frac{4\pi Z_1 e}{2L+1}\left[B(EL)\uparrow\right]^{1/2}\frac{1}{r^3} & \text{for } r > R_C, \\ \frac{4\pi Z_1 e}{2L+1}\left[B(EL)\uparrow\right]^{1/2}\frac{r^2}{R_C^5} & \text{for } r \leq R_C. \end{cases}$$

The nuclear part of the form factor was calculated within the framework of the collective model:

$$F_L^N(r) = \left(\beta_L^N\ R^*\ V\frac{df(r)}{dr} + i\beta_L^N\ R'^*\ W\frac{dg(r)}{dr}\right), \tag{9}$$

with

$$R^* = r_0\ A^{*1/3}, \tag{10}$$

$$R'^* = r_0'\ A^{*1/3}, \tag{11}$$

where A^* is the mass of the nucleus (target or projectile) which gets excited in the inelastic collision.

TABLE I. Optical-model parameters.

Projectile	E_{lab} (MeV)	V (MeV)	r (fm)	a (fm)	W (MeV)	r' (fm)	a' (fm)	Analysis
^{18}O	49	67	1.04	0.857	10.6	1.32	0.591	optical model
^{18}O	29–46	67	1.04	0.857	10.6	1.32	0.591	optical model
^{18}O	49	67	1.04	0.893	7.5	1.32	0.626	coupled channels
^{16}O	30.5–46	131.6	1.22	0.500	8.2	1.22	0.500	optical model

The parameters in the radial form factor are the same as those in the corresponding entrance channel optical potentials. The $B(E2)$ value for ^{64}Zn used in the calculations was determined from data obtained at energies below the Coulomb barrier which are considered "safe" for a Coulomb excitation experiment [11]. The $B(E2)$ value for ^{18}O was taken from Ref. [25]. The nuclear deformation parameters β_L^N were treated as free parameters.

The data were analyzed in the coupled-channels approach also employing the PTOLEMY computer code in its version which can compute heavy-ion inelastic scattering cross sections with the coupled-channels formalism [21, 22]. The form factors were the same as those for the DWBA analysis. Because of the strong coupling between the elastic and inelastic channels, the optical-model parameters used for the DWBA calculations had to be modified to fit simultaneously the elastic and the inelastic data. In the coupled-channels calculations the nuclear deformation parameters β_L^N were also treated as free parameters and the $B(E2)$ values were the same as used in the DWBA calculations.

IV. RESULTS AND DISCUSSION

The optical-model parameters used in the calculations are presented in Table I. The reduced electric transition probability values and the nuclear deformation parameters used in the analysis are presented in Table II. A good agreement is observed between the experimental elastic scattering data and the theoretical predictions (see Figs. 5, 6, and 7).

The angular distributions for ^{18}O inelastic scattering for the target and for the projectile excitation are presented in Fig. 5. The curves represent the results from DWBA (dashed line) and coupled-channels (solid line) calculations with the parameters given in Tables I and II and with the couplings shown in Fig. 5. A good agreement between experimental data and theoretical predictions for the target excitation at forward angles is obtained with the $B(E2)$ value extracted from the reorientation effect measurement [11] in Coulomb excitation for the first 2^+ state of ^{64}Zn. For the Coulomb-nuclear interference region and at backward angles, the DWBA calculation overpredicts the cross sections whereas the coupled-channels calculation presents a good fit to the data.

The angular distribution for the excitation of the first 2^+ state in ^{18}O (Fig. 5) shows a pronounced Coulomb-nuclear interference minimum. The magnitude of the cross sections and the amplitude of the oscillations in the DWBA predictions are in reasonable agreement with the experimental data. However, the interference minimum is shifted towards larger angles by $\sim 5°$ (c.m.) with respect to the data. A similar effect has been reported for other systems [2–10]. Coupled-channels calculations taking into account the transitions shown in Fig. 5 were performed with the parameters of Tables I and II. Couplings leading to mutual excitation of both target and projectile were not considered. In these calculations the interference minimum is shifted toward forward angles by $\sim 1.5°$ with respect to the DWBA calculations. This shift, however, is not large enough to reproduce the experimental results.

In order to reproduce in the coupled-channels calculations the position of the experimental interference minimum, it was found necessary to use a value for the quadrupole moment of the first 2^+ state of ^{18}O which is 10 times larger than the experimental value. Such large value is not physically acceptable and the calculations done with it underpredict the cross sections at backward

TABLE II. Nuclear and Coulomb deformation parameters used in the calculations.

Reaction	β_2^N	$\beta_2^N R$ (fm)	$B(E2)\uparrow$ (e^2 b^2)	$\beta_2^{C\,a}$	$\beta_2^C R_C{}^a$	Analysis
^{18}O+^{64}Zn(2^+)	0.301	1.25	0.168[b]	0.229	1.14	DWBA
^{18}O(2^+)+^{64}Zn	0.367	1.00	0.0039[c]	0.305	1.00	DWBA
^{18}O+^{64}Zn(2^+)	0.275	1.14	0.168	0.229	1.14	coupled channels
^{18}O(2^+)+^{64}Zn	0.367	1.00	0.0039	0.305	1.00	coupled channels
^{16}O+^{64}Zn(2^+)	0.256	1.25	0.168	0.229	1.14	DWBA

[a] $B(E2)\uparrow = \left[\frac{3}{4\pi} ZeR_C\right]^2 \left[\beta_2^C R_C\right]^2$, $R_C = 1.25A^{1/3}$ (fm).

[b] Reference [11].

[c] Reference [25].

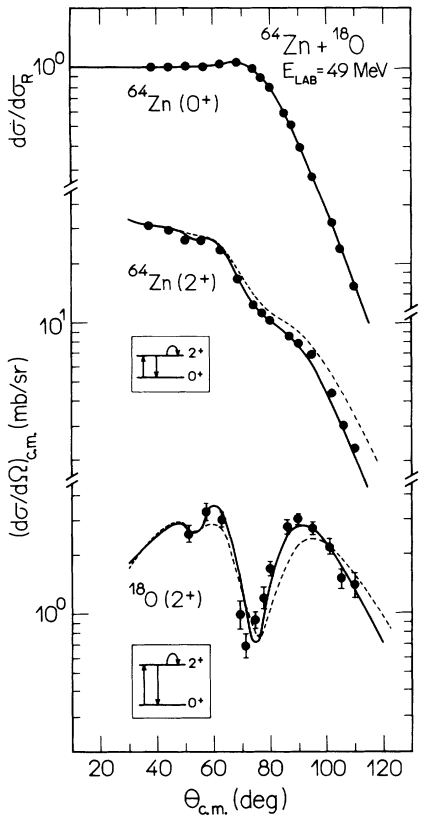

FIG. 5. Angular distributions for the elastic and inelastic scattering of ^{18}O from ^{64}Zn measured at E_{lab} = 49 MeV. The solid curves result from coupled-channels calculations with the coupling schemes shown in the inserts. The dashed lines are the result from DWBA calculations. The theoretical cross sections were obtained using the parameters presented in Tables I and II.

angles. This is in line with results that have previously been reported for other systems [2, 3]. The effect of including higher 2^+ and 4^+ states in coupled-channels calculations is also too small to explain the shift, as observed before [2].

Earlier attempts based on *ad hoc* changes in the geometry of the nuclear form factor were able to reproduce the observed shift of the angular distributions. Such procedure, however, resulted in discrepancies in fitting excitation functions measured at backward angles [4]. Also *ad hoc* variations of the phase of the nuclear form factor [4] and changes in the distorting potential [7] have been shown to produce ^{18}O (2^+) angular distributions in qualitative agreement with the experimental data. None of these arbitrary parameter variations have been adopted in the present work.

Of previous attempts to explain the ^{18}O projectile excitation [2–10], only a semimicroscopic approach in which the interaction is represented by a collective core plus valence terms (obtained with a microscopic single-folding model [8]) leads to reasonable results when compared to the experimental data for the excitation of the 2^+ state in ^{18}O [8, 9]. But it is difficult to interpret these results because there is a large number of parameters involved in the calculations. In a microscopic analysis [10] of the inelastic scattering of ^{18}O from ^{64}Ni [4] employing real double-folded and imaginary Woods-Saxon interaction potentials, it was found that *ad hoc* adjustments of the imaginary potential and form factor are needed to reproduce the Coulomb-nuclear interference pattern observed in the data. The real part of the potential affects only the magnitude of the calculated cross sections. Thus, arbitrary changes in the phenomenological parameters of the interaction potential and of the form factor have been required up to now in order to bring the theoretical calculation into agreement with the experimental data, reflecting the lack of a theoretical model which describes the ^{18}O projectile excitation in an unambiguous way.

The optical-model calculations for the ^{18}O elastic scattering excitation function, using the parameters of Table I, are in good agreement with the experimental data (Fig. 6). The theoretical predictions for the ^{18}O inelastic excitation function with target excitation is also in good agreement with the experimental data for energies where the Coulomb interaction is predominant and in the Coulomb-nuclear interference region. For energies above E_{lab} = 43 MeV, the calculations overpredict the experi-

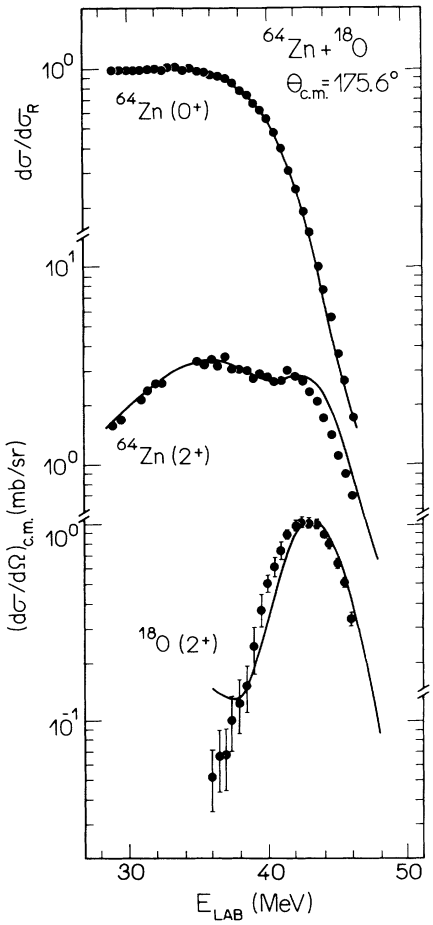

FIG. 6. Excitation functions for the elastic and inelastic scattering of ^{18}O from ^{64}Zn measured at $\theta_{c.m.}$ = 175.6°. The solid curves result from optical model (elastic) and from DWBA (inelastic) calculations with the parameters presented in Tables I and II.

mental inelastic scattering cross sections (Fig. 6). A reasonable agreement between experiment and theory is obtained for the inelastic scattering excitation function involving projectile excitation for energies above $E_{lab} = 38$ MeV (Fig. 6).

The excitation functions for the ^{16}O scattering are presented in Fig. 7. A good fit to the elastic scattering was obtained with the optical-model parameters presented in Table I. The inelastic scattering data for the excitation of the first 2^+ state of ^{64}Zn is reasonably well described by DWBA calculations with the deformation parameters of Table II. However, the amplitude of the interference minimum is not well reproduced by the theoretical calculations. In order to fit the interference minimun data, the imaginary potential was allowed to vary. The solid curve in Fig. 7 represents the best fit obtained to the inelastic scattering data using optical-model parameters which also give a good fit to the elastic scattering data. This result is in line with what was observed in the excitation function of the inelastic scattering of ^{16}O by ^{92}Zr [26]. There it was seen that changes in the reorientation coupling with the incident energy could deepen the interference minimum; however, further experimental information would be required to definitely conclude what was changing with the incident energy.

Threshold "anomalies" are known to occur around the Coulomb barrier [27]. Concerning optical potentials, these anomalies consist of an increase in the strength of the real potential when the energy drops down to the Coulomb barrier, accompanied by a decrease in the strength of the imaginary potential which reflects the closing of nonelastic channels at sub-barrier energies. In our analysis of the excitation functions the parameters were kept constant through the whole energy range, since data were available only at one angle. The effect of using constant parameters in the elastic scattering is small. But the inability to properly fit the interference minimum in the ^{64}Zn (2^+) inelastic excitation function may be an indication that some parameters might be changing with energy.

The excitation functions for ^{16}O and ^{18}O projectiles (Figs. 8 and 9) present some significant differences. Since the Coulomb form factors are essentially the same for both ions, these results point to differences in the nuclear contributions in the interaction of ^{16}O and ^{18}O projectiles with the ^{64}Zn target. The ^{18}O elastic scattering cross section deviates from the Rutherford cross section at a lower center-of-mass energy than that found for ^{16}O elastic scattering (see Fig. 8). This result might reflect the fact that, since ^{18}O has a smaller binding energy, the $^{18}O + {}^{64}Zn$ system has a larger number of open channels than the $^{16}O + {}^{64}Zn$ system at a given energy.

At low bombarding energies, the inelastic excitation functions for ^{16}O and ^{18}O follow pure Coulomb excitation (see Fig. 9) and the calculated cross sections are not sensitive to the optical model and the nuclear deformation parameters. In this energy range the DWBA cross sections depend essentially on the $B(E2)$ value. The excellent agreement of the sub-Coulomb data with the calculated cross sections for both ions gives support to the

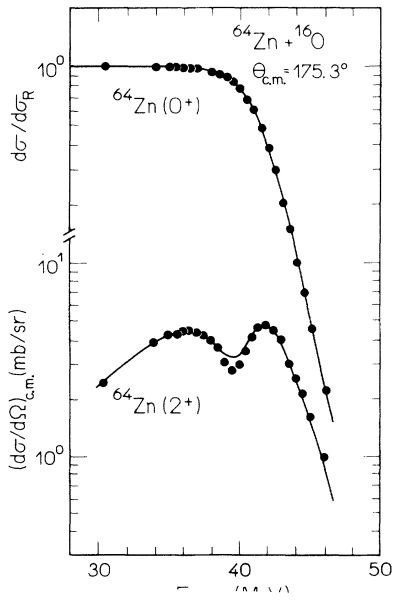

FIG. 7. Excitation functions for the elastic and inelastic scattering of ^{16}O from ^{64}Zn measured at $\theta_{c.m.} = 175.3°$. The solid curves are the results of optical model (elastic) and DWBA (inelastic) calculations with the parameters given in Tables I and II.

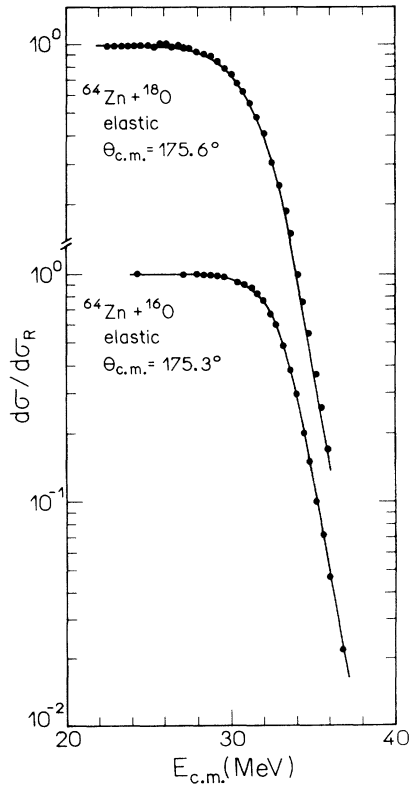

FIG. 8. Excitation functions for the elastic scattering of ^{18}O and ^{16}O from ^{64}Zn measured at backward angles. The solid curves are theoretical calculation results with the optical model parameters presented in Table I.

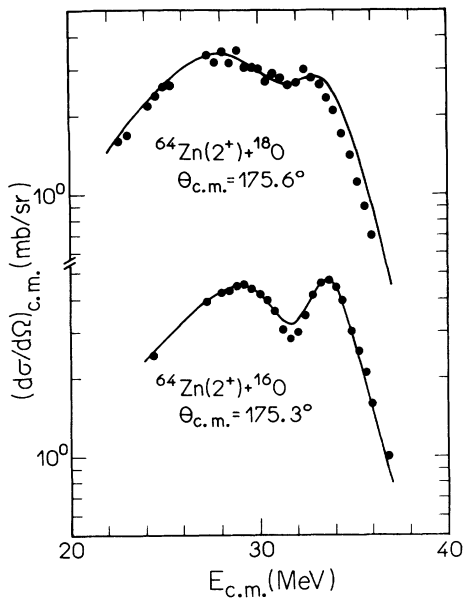

FIG. 9. Excitation functions for the inelastic excitation of the lowest 2^+ state in ^{64}Zn by ^{18}O and ^{16}O. The solid curves are the results of DWBA calculations with the parameters given in Tables I and II.

$B(E2)$ value for the first 2^+ state of ^{64}Zn obtained in Coulomb excitation measurements [11]. At higher energies the inelastic cross sections fall off rapidly for both projectiles and the DWBA results are strongly dependent on the optical-model and nuclear deformation parameters.

Good fits to the ^{16}O and ^{18}O inelastic excitation functions of the first 2^+ state of ^{64}Zn could be achieved in both cases with the same $\beta_2^N R$ value (see Table II). This could indicate that the assumed mechanism with a collective form factor is an acceptable description for the excitation of the first 2^+ state of ^{64}Zn by ^{16}O and ^{18}O inelastic scattering.

A sharp difference in the inelastic ^{64}Zn (2^+) excitation functions for ^{16}O and ^{18}O projectiles was observed in the Coulomb-nuclear interference energy region. While the interference minimum has a large amplitude in the case of the ^{16}O projectile, there is no pronounced minimum for the ^{18}O case. This effect has been previously observed for other targets [28]. Such difference might indicate that there are relevant contributions to the nuclear interaction from the two valence neutrons of ^{18}O and that these degrees of freedom should explicitly be taken into account in the description of the excitation processes.

ACKNOWLEDGMENTS

The authors would like to thank all members of LIP-IFUSP for their assistance during the experiment. This work was supported in part by Conselho Nacional de Desenvolvimento Científico e Tecnológico (CNPq), by Financiadora de Estudos e Projetos (FINEP), and by Fundação de Amparo à Pesquisa do Estado de São Paulo (FAPESP).

[1] G. R. Satchler, *Direct Nuclear Reactions* (Oxford University Press, Oxford, 1983).
[2] F. Videbaeck, P. R. Christensen, O. Hansen, and K. Ulbak, Nucl. Phys. **A256**, 301 (1976).
[3] J. Carter, R. G. Clarkson, V. Hnizdo, and J. P. F. Sellschop, Nucl. Phys. **A297**, 520 (1978).
[4] K. E. Rehm, H. J. Körner, M. Richter, H. P. Rother, J. P. Schiffer, and H. Spieler, Phys. Rev. C **12**, 1945 (1975).
[5] H. Essel, K. E. Rehm, H. Bohn, H. J. Körner, and H. Spieler, Phys. Rev. C **19**, 2224 (1979).
[6] D. C. Uhlhorn, B. Gonsior, D. Wegner, K. P. Lieb, H. H. Wolter, and A. M. Kleinfeld, Z. Phys. A **311**, 79 (1983).
[7] A. J. Baltz and S. Kahana, Phys. Rev. C **17**, 555 (1978).
[8] S. Landowne, R. Schlicher, and H. H. Wolter, Nucl. Phys. **A373**, 141 (1982).
[9] E. E. Gross, J. R. Beem, K. A. Erb, M. P. Fewell, D. Shapira, M. J. Rhoades-Brown, and G. R. Satchler, Nucl. Phys. **A401**, 362 (1983).
[10] S. P. Van Verst and K. W. Kemper, Phys. Rev. C **36**, 628 (1987).
[11] S. Salém-Vasconcelos, M. J. Bechara, J. H. Hirata, and O. Dietzsch, Phys. Rev. C **38**, 2439 (1988).
[12] J. H. Hirata, M.Sc. thesis, University of São Paulo, 1975 (unpublished).
[13] M. Samuel (unpublished).
[14] Z. Berant, R. A. Eisenstein, Y. Horowitz, U. Smilansky, and P. N. Tandon, Nucl. Phys. **A196**, 312 (1972).
[15] J. E. Spencer and H. A. Enge, Nucl. Instrum. Methods **49**, 181 (1967).
[16] E. R. Cruz, M.Sc. thesis, University of São Paulo, 1978 (unpublished).
[17] K. Koide, A. Bairrio-Nuevo, Jr., H. Takai, B. Marechal, and O. Dietzsch, Nucl. Instrum. Methods **215**, 177 (1983).
[18] H. Takai, Ph.D. thesis, Federal University of Rio de Janeiro, 1986.
[19] E. H. Auerbach, Comput. Phys. Commun. **15**, 165 (1978).
[20] D. H. Gloeckner, M. H. Macfarlane, and S. C. Pieper, Argonne National Laboratory Report No. ANL-76-11, 1978 (unpublished).
[21] M. Rhoades-Brown, M. H. Macfarlane, and S. C. Pieper, Phys. Rev. C **21**, 2417 (1980).
[22] M. Rhoades-Brown, M. H. Macfarlane, and S. C. Pieper, Phys. Rev. C **21**, 2436 (1980).
[23] P. R. Christensen, V. I. Manko, F. D. Becchetti, and R. J. Nickles, Nucl. Phys. **A207**, 33 (1973).
[24] L. West, Jr. and N. R. Flecher, Phys. Rev. C **15**, 2052 (1977).
[25] M. P. Fewell, A. M. Baxter, D. C. Kean, R. H. Spear, and T. H. Zabel, Nucl. Phys. **A321**, 457 (1979).
[26] E. M. Takagui, G. R. Satchler, H. Takai, K. Koide, and O. Dietzsch, Nucl. Phys. **A514**, 120 (1990).
[27] G. R. Satchler, Phys. Rep. **199**, 147 (1991).
[28] E. C. Pollacco, C. Garrett, and D. C. Weisser, Phys. Rev. C **19**, 2073 (1979).